Carbohydrate Polymers 87 (2012) 830–838

Contents lists available at SciVerse ScienceDirect

Carbohydrate Polymers

journal homepage: www.elsevier.com/locate/carbpol

Effects of external factors on the arrangement of plate-liked Fe_2O_3 nanoparticles in cellulose scaffolds

Shilin Liu [a,b,*], Ran Li [a], Jinping Zhou [a], Lina Zhang [a,**]

[a] Department of Chemistry, Wuhan University, Wuhan 430072, China
[b] College of Chemical and Material Engineering, Jiangnan University, Wuxi, Jiangsu 214122, China

ARTICLE INFO

Article history:
Received 21 July 2011
Received in revised form 16 August 2011
Accepted 23 August 2011
Available online 30 August 2011

Keywords:
Cellulose
Fe_2O_3 nanoparticles
Anisotropy
Magnetic

ABSTRACT

To clarify the effects of the external factors on the alignment of the plate-like Fe_2O_3 nanoparticles in the cellulose matrix, different preparation methods under various conditions including low temperature, static and rotating magnetic, as well as uniaxial drawing were performed in present work. The results indicated that Fe_2O_3 nanoparticles synthesized in the cellulose scaffolds were randomly distributed before drying. A weak static and rotating magnetic field led to different alignments of the Fe_2O_3 nanoparticles in the cellulose matrix. Moreover, the uniaxial drawing of the composite films destroyed the regular distribution of the Fe_2O_3 nanoparticles, leading to the changing of the morphology of the nanoparticles from plate-like to rod-like. The interesting results revealed that the magnetic properties of the composite films could be controlled by modulating the alignment of the Fe_2O_3 nanoparticles in the cellulose scaffolds, which was very fascinating for the preparation of magnetic composite materials with controlled properties.

© 2011 Elsevier Ltd. All rights reserved.

1. Introduction

Composites with aligned structures are of interests in a wide range of applications such as organic electronics (Gu, Zheng, Zhang, & Xu, 2004), microfluidics (Quake & Scherer, 2000), molecular filtration (Yamaguchi et al., 2004), nanowires (Adelung et al., 2004), and tissue engineering (Baker, Nathan, Gee, & Mauck, 2010; Chen, Yang, Ma, & Wu, 2011). The aligned structure of the composites often has anisotropic properties (Akima et al., 2006; Bliznyuk et al., 2005; Kim, 2005; Prasse, Cavaille, & Bauhofer, 2003; Shi et al., 2005; Tai, Wu, Tominaga, Asai, & Sumita, 2005; Tezvergil, Lassila, & Vallittu, 2003). The alignment of an object in a polymer matrix has attracted much attention. It has been reported that electric field is an effective route to make materials with an aligned structure, and it has been successfully accomplished with a variety of different structures including nanoparticles (Bezryadin, Dekker, & Schmid, 1997), nanowires (Smith et al., 2000), fibers (Takahashi, Murayama, Higuchi, Awano, & Yonetake, 2006), layered silicates (Koerner, Jacobs, Tomlin, Busbee, & Vaia, 2004), and carbon nanotubes (Chen, Saito, Yamada, & Matsushige, 2001; Kamat et al., 2004; Martin et al., 2005). Homogeneous magnetic field was also used to achieve controlled orientation of particles in polymer matrixes, and these oriented particles made the composite materials had anisotropy properties (Eguchi, Angelone, Yennawar, & Mallouk, 2008; Majewski, Gopinadhan, Jang, Lutkenhaus, & Osuji, 2010; Porion, Faugère, Michot, Paineau, & Delville, 2010; Shaver et al., 2009; Wang et al., 2011). Shear stress was another field that could effectively promote orientation of the dispersed particles in polymer nanocomposites, and could produce long-range in-plane order quickly (Angelescu et al., 2004; Dykes, Torkelson, Burghardt, & Krishnamoorti, 2010; Hong, Adamson, Chaikin, & Register, 2009). Compared with the orientation of spherical and one-dimensional objects in polymer matrix, little attention has been paid on the alignment of two-dimensional shaped (such as plate-like) magnetic nanoparticles in a polymer matrix. This is a more complicated process for the investigation of the magnetic nanoparticles with inherent magnetic and morphological anisotropies in a polymer matrix.

In our previous work, a facile method for the synthesis of magnetic iron oxide nanoparticles in the cellulose matrix was developed, and magnetic cellulose composite materials such as films (Liu, Zhou, & Zhang, 2011a, 2011b; Liu, Zhou, Zhang, Guan, & Wang, 2006; Zhou et al., 2009), fibers (Liu, Zhang, Zhou, & Wu, 2008; Liu, Zhang, Zhou, Xiang, et al., 2008), and microspheres (Luo, Liu, Zhou, & Zhang, 2009; Luo & Zhang, 2009b, 2010) with novel properties were prepared successfully. Interestingly, the synthesized Fe_2O_3 nanoparticles in the cellulose films were plate-

* Corresponding author at: Department of Chemistry, Wuhan University, Wuhan 430072, China. Tel.: +86 027 87219274; fax: +86 027 68762005.
** Corresponding author. Tel.: +86 027 87219274; fax: +86 027 68762005.
E-mail addresses: slliu2009@jiangnan.edu.cn (S. Liu), lnzhang@public.wh.hb.cn (L. Zhang).

0144-8617/$ – see front matter © 2011 Elsevier Ltd. All rights reserved.
doi:10.1016/j.carbpol.2011.08.069

like, and they were self-aligned regularly in the cellulose matrix when it was dried at ambient conditions, leading to the composite films exhibit obvious magnetic anisotropy. This result was totally different from those reported works about the preparation of orientated distribution of inorganic in polymer matrix, and the distribution of inorganic nanoparticles in polymer matrix was often randomly. It is well known that exterior force field was often must be applied for any attempt to align inorganic components in a polymer matrix. In order to clarify this interesting phenomenon, different conditions including low temperature, static and rotating magnetic, as well as uniaxial drawing have been used for the preparation of the Fe_2O_3/cellulose composite films in present work. The effects of a weak static magnetic field and rotating magnetic field on the distributions of the Fe_2O_3 nanoparticles were investigated by transmission electron microscopy (TEM), HRTEM, and superconducting quantum interference device (SQUID). This work provided useful information dealing with changing the morphology of Fe_2O_3 nanoparticles and rearranging Fe_2O_3 nanoparticles inside the cellulose films by controlling the conditions outside.

2. Experimental

2.1. Materials

Cotton linter pulp (α-cellulose >95%) was provided by Hubei Chemical Fiber Group Co., Ltd. (Xiangfan, China), its viscosity-average molecular weight (M_η) was determined to be 1.33×10^5. Other chemical reagents with analytical grade were supplied by the Sinopharm Chemical Reagent Co., Ltd. (China) and used without further purification.

2.2. Preparation of composite films

Cellulose (cotton linter pulp) was dissolved directly by using NaOH/urea aqueous solution pre-cooled to −12 °C. The obtained cellulose solution (4 wt%) was centrifuged at 8000 rpm for 20 min at about 15 °C for degasification, and then cast on a glass plate and immersed into 5 wt% H_2SO_4 solution (2 L) for 5 min to coagulate and regenerate. The regenerated cellulose films were washed with deionized water for many times to remove other impurities. Then the films were immersed into aqueous $FeCl_2$ solution (0.5 M) for 24 h, and subsequently were treated with aqueous NaOH solution (4 M) for 20 min, followed by washing with deionized water for several times. To investigate the influence of different conditions on the morphology and distribution of the Fe_2O_3 nanoparticles that were synthesized in the cellulose films, different drying processes were carried out as follows.

2.2.1. Freeze-drying method

After being washed with deionized water, the obtained swollen composite film after being washed with deionized water was immersed into liquid nitrogen to quench and then freeze-dried.

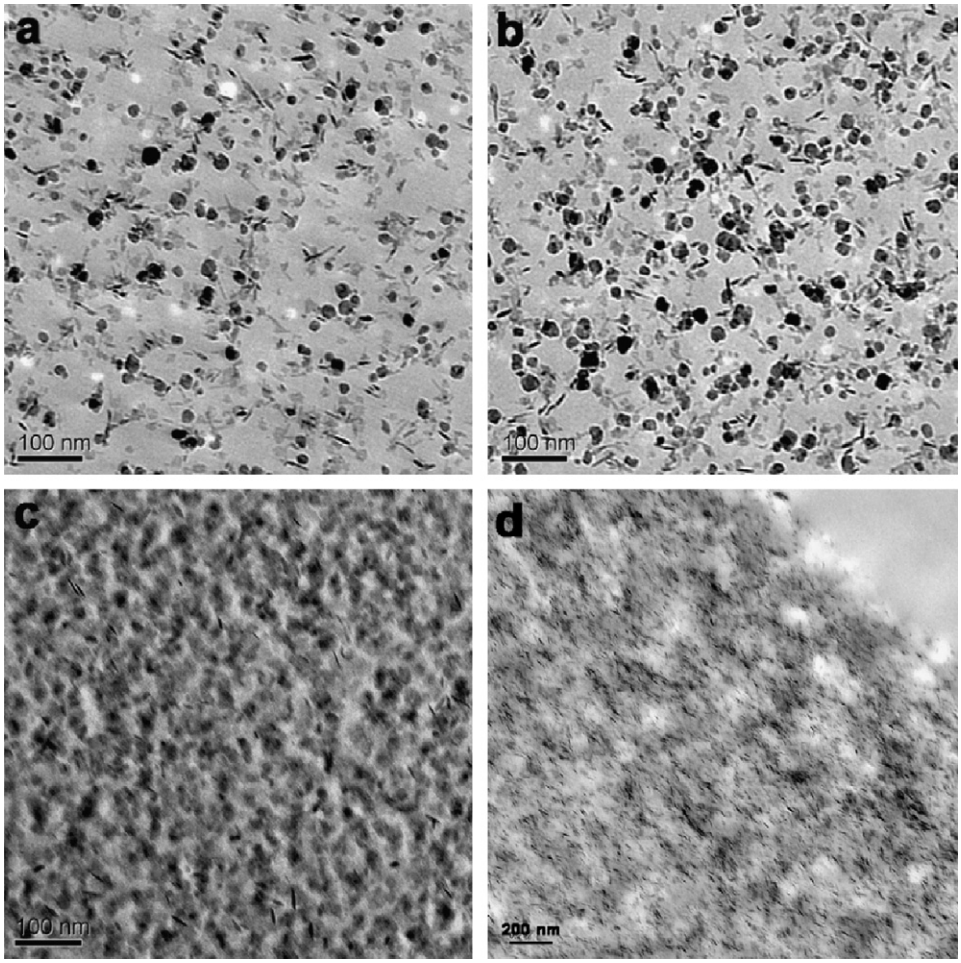

Fig. 1. TEM images of the composite film prepared by freeze-dried (a and b) and being dried at ambient conditions (c and d). (a and c) The slice was parallel to the film plane and (b and d) the slice was perpendicular to the film plane.

2.2.2. Dried under a static magnetic field

After being washed with deionized water, the obtained swollen composite film was fixed on a PMMA plate, and then put in the middle of two magnets and dried at room temperature. The surface of the composite film was perpendicular to the magnetic field direction. The magnetic field intensity in the center of the composite film was about 600 Oe that tested by using a magnetomer.

2.2.3. Dried under a rotating magnetic field

After being washed with deionized water, the obtained swollen composite film was fixed on a PMMA plate, and then putted on a magnetic stirring and turned the stirring speed to the maximum, finely dried at room temperature. The magnetic field intensity in the center of the composite film was about 600 Oe that tested by using a magnetomer.

2.2.4. Dried under uniaxial drawing

The wet composite film was drawn to different draw ratios (DR = final film length/starting length) as follows. The wet composite film was cut into strips with 40 mm × 120 mm and then clamped in a stretching device controlled by a computer and dried at ambient temperature. The draw ratios of the drawn films ranged from 1 to 1.22. Draw ratios greater than 1.22 could not be obtained because the composite film would be broken during the drying process. The drawn composite films with DR = 1.04, 1.16 and 1.22 were coded as DR = 1.04, DR = 1.16 and DR = 1.22, respectively.

2.3. Characterization

Transmission electron microscopy (TEM) images were carried out on a JEOL JEM-2010 (HT) electron microscope with an accelerating voltage of 200 kV. The magnetic properties of the composite films were characterized by using superconducting quantum interference device (SQUID) at 298 K, and the hysteretic loops were obtained in a magnetic field varied from −7.5 T to +7.5 T.

3. Results and discussion

The crystallite phase of the plate-like Fe_2O_3 nanoparticles that were in situ synthesized in the cellulose scaffolds was γ-Fe_2O_3, as well as the structure and properties of the composite film have been investigated in our previous works (Liu et al., 2006, 2011a, 2011b). Interestingly, the Fe_2O_3 nanoparticles were self-aligned regularly in the cellulose matrix, and the composite films had an obvious magnetic anisotropy. It was totally different from the reported works about the preparation of inorganic/polymer nanocomposites. For most researchers Fe_2O_3 nanoparticles were tried to make the inorganic components aligned in the polymer matrix through various methods. Preliminary explanation of this interesting phenomenon would correlate to the different shrinkage of the composite film in two directions. When the Fe_2O_3 nanoparticles synthesized in the porous matrix, during the drying process, the shrinkage of the composite film in the longitudinal direction was more prominent than that happened in the transverse direction, for the composite film was fasted during the drying process. The cellulose microfibrils shrank in the longitudinal direction would induce the Fe_2O_3 nanoparticles distributed regularly in cellulose matrix. To furthermore clarify it, the prepared composite film after being washed with water was immersed into liquid nitrogen quickly to quench and then freeze-dried. Fig. 1a and b shows the TEM images of the composite film. In the slices that parallel and perpendicular to the surface of the composite film, circular and needle-like Fe_2O_3 nanoparticles were observed, and their distributions in the cellulose matrix was randomly, which was obviously different from that in the composite film that dried at ambient conditions, as shown in Fig. 1c and d. There was little change in the morphology and particle size of the Fe_2O_3 nanoparticles in the composite films prepared by freeze-drying and natural drying. The Fe_2O_3 nanoparticles synthesized in the porous structured cellulose films at wet state were plate-like, and their distributions were random.

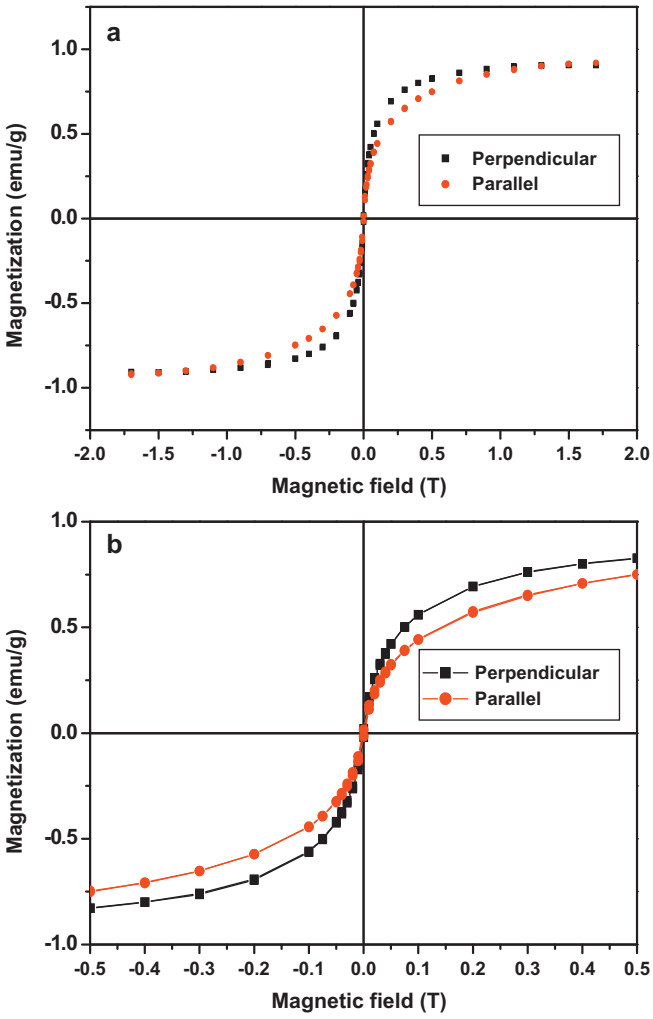

Fig. 2. Hysteresis loops of the freeze-dried composite film measured at T = 298 K. (a) Full hysteresis loop, (b) the hysteresis loop between −500 and 500 Oe expanded.

Fig. 2 shows the magnetic hysteresis curves of the composite film prepared by freeze-drying. The randomly distributed Fe_2O_3 nanoparticles in the composite films had different magnetic properties. The magnetization of the composite films increased with an increase of the applied field. The composite films exhibited typical superparamagnetic behavior without hysteresis loops, and the coercivity was nearly zero. This phenomenon could be ascribed to the small particle size and weak magnetic properties of the Fe_2O_3 nanoparticles. The diameters of the magnetic nanoparticles synthesized in the cellulose matrix were smaller than the critical size (30–50 nm) of the Fe_2O_3 single domains (Goya, Berquo, Fonseca, & Morales, 2003). It is well known that magnetic particles with particle size smaller than the critical particle diameter can be called as single domains. As the particle size continues to decrease below the single domain value, the particles exhibit superparamagnetic properties, that is, no hysteresis. Moreover, the magnetic anisotropy behavior of the composite film was hardly to be detected, and there was little difference in the magnetic properties of the composite film when the testing direction that was parallel or perpendicular to the magnetic field. This was different from that of the composite

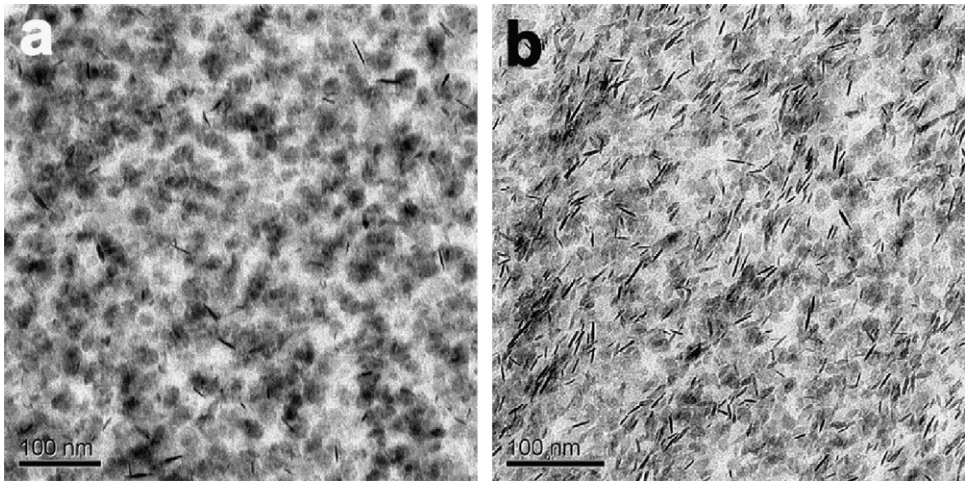

Fig. 3. TEM images of the composite film fixed on a PMMA plate with a static magnetic field and air-dried. (a) The slice was parallel to the film plane and (b) the slice was perpendicular to the film plane.

film prepared by natural drying. Based on the results of the composite films prepared by freeze-drying and natural drying, it could be concluded that there was a rearrangement of the Fe_2O_3 nanoparticles in the composite film during the drying process at ambient conditions.

In order to testify this conclusion, a weak static magnetic field was applied during the drying process of the composite film at ambient conditions, and the detailed process was described in Section 2. Fig. 3 shows the TEM images of the surface and cross-section of the composite film. In the slice plane that was parallel to the surface of the composite film, the morphology of the Fe_2O_3 nanoparticles was mainly acicular with irregular morphology, and a small quantity of needle-like nanoparticles was also detected. While in the slice plane that was perpendicular to the surface of the composite film, Fe_2O_3 nanoparticles with needle-like and irregular circular morphologies were coexisted. There was little change in the morphology of the synthesized nanoparticles, except for their distributions and slight increase in the thickness of the nanoparticles. The distribution of the Fe_2O_3 nanoparticles in the cellulose matrix was regular. It would be ascribed to the combined interactions of magnetic field and shrinkage of the cellulose matrix. It has been reported that magnetic nanoparticles often have one or multi-easy magnetic axis, and they would align with the magnetic field lines direction in the presence of an external magnetic field (Kimura, Yamato, Koshimizu, Koike, & Kawai, 2000). During the drying process, the magnetic nanoparticles in the cellulose scaffolds would rearrange to the external magnetic field direction, and the shrinkage of the cellulose matrix would also induce them to lie low for the minimum energy principle. The result indicated that external force field had an influence on the distribution of the Fe_2O_3 nanoparticles during the drying process of the composite film.

Magnetic behavior of the composite film supported the conclusion, as it was shown in Fig. 4. By changing the testing direction, it was possible to distinguish the magnetic anisotropy properties of the composite film. The observed hysteresis loop of the composite film was slanted in the perpendicular testing direction. Moreover, the remanence was only 1.14% of the saturation magnetization, while in the parallel testing direction, it was 2.4% of the saturation magnetization. It was a direct evidence of a magnetic anisotropy of the composite film. The observed anisotropy was analogous to the magnetic crystal anisotropy that was typically associated with magnetic thin films, and shape anisotropy was also played an important role in it. The magnetic film that tested in the perpendicular direction of the applied magnetic field, the

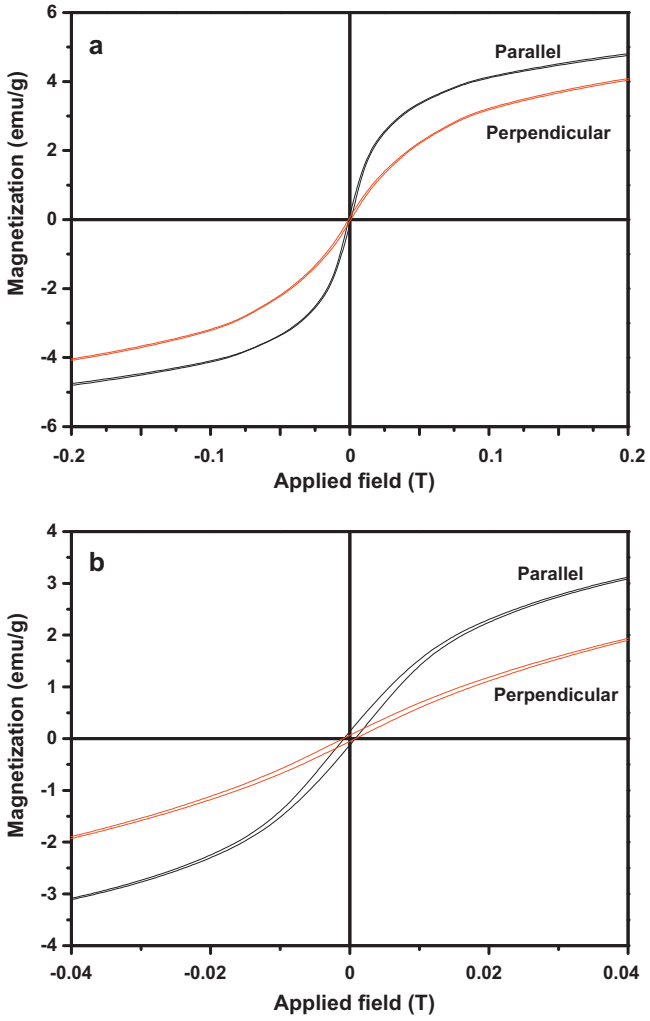

Fig. 4. Hysteresis loops of the air-dried composite film fixed on a PMMA plate with a static magnetic field measured at $T = 298$ K. (a) Full hysteresis loop and (b) the hysteresis loop between −400 and 400 Oe expanded.

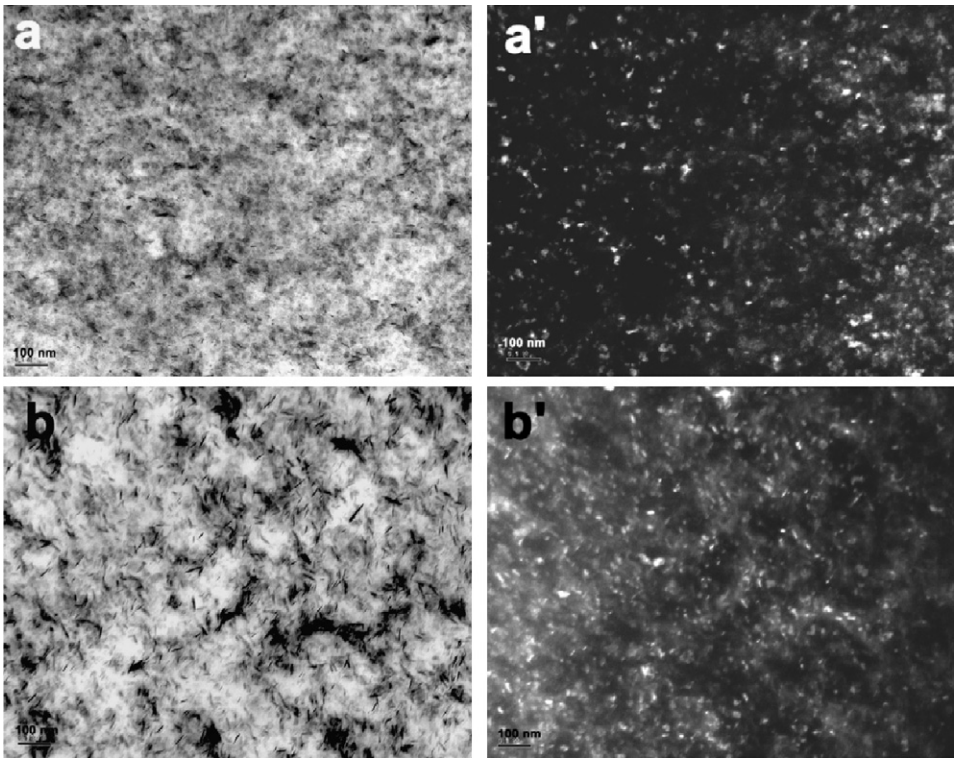

Fig. 5. TEM images of the composite film dried on a rotating magnetic field at room temperature. (a and a′) The slice was parallel to the film plane and (b and b′) the slice was perpendicular to the film plane.

perpendicular field needed to compensate for the demagnetization field before saturating the film, whereas for an in plane field testing direction, it did not need. Thus, the saturation field in the perpendicular testing direction was higher than that in parallel testing direction. The composite film investigated here behaved diverse magnetic behavior, which would be resulted from the strong dipole–dipole interactions of the adjacent magnetic nanoparticles. It has been reported that there was considerably large dipole-field anisotropy in Fe_2O_3 nanoparticles, and it could cause comparably large uniaxial anisotropy even without spin–orbit contribution (Yanagihara, Hagiwara, Najazumi, & Kita, 2007). When the magnetic moments of all the particles were aligned by an in-plane field applied parallel to the composite film, the moment of a particle was stabilized by the vector sum of the dipole fields from all its neighbors. When the magnetic moments of all the particles were aligned by an out-of-plane field applied perpendicular to the composite film, the dipole field from one particle to another always tended to destabilize the moment. The vector sum was increased, and more energy was needed to overcome the dipolar field before aligning the moments. Nonetheless, this difference in saturation field was in good agreement with the observed anisotropy seen in Fig. 4b.

It has been reported that the easy magnetization axis would be aligned in the direction of the applied magnetic field when the magnetic alignment was carried out under a static magnetic field, and while under a rotating magnetic field, the hard magnetization axis (χ_3) would align in the direction perpendicular to the plane of the applied rotating magnetic field. In order to further testify the rearrangement of the magnetic nanoparticles in the composite films during the drying process at ambient condition, a rotating magnetic field was applied during the drying process. Fig. 5 shows the TEM images of the surface and cross-section of the composite film. Interestingly, the morphology of the observed nanoparticles mostly was needle-like in the slice planes that parallel or perpendicular to the surface of the composite film. It was noted that the width of the needle-like nanoparticles was larger than that in the composite films prepared by natural and freeze-drying, as well as dried under a static magnetic field. Moreover, their alignment in the composite film was also different. The co-existed irregular acicular morphology suggested that the resulting magnetic nanoparticles were plate-like. The most likely alignment of the magnetic nanoparticles was that all the nanoparticles were nearly stand up in the composite film. This phenomenon of distributions of the magnetic nanoparticles under a static or rotating magnetic field could be forecasted based on magnetic theory, which has been demonstrated experimentally by Kimura and coworkers firstly (Kimura, Kimura, & Yoshino, 2006; Kimura & Yoshino, 2005; Kimura, Yoshino, Yamane, Yamato, & Tobita, 2004). They reported the theoretical and experimental results of the motion of the two dimensional particle with $\chi_3 < \chi_2 = \chi_1$ exposed to a magnetic field circularly rotating on the xy plane. The motion of this particle in the rotating regime was deduced by using the following equation (Kimura et al., 2004):

$$\frac{d_\theta}{d_t} = (2\tau)^{-1} \cos^2(\varphi - \omega t) \sin 2\theta$$

$$\frac{d\varphi}{dt} = -(2\tau) \sin^2(\varphi - \omega t)$$

The magnetic field $\boldsymbol{B}$ was rotating on the xy plane at the angular velocity of ω (rad/s), for simplicity, assumed $\varphi = 0$ and took the limit of $\omega\tau \to \infty$, the following formula was obtained:

$$\tan\theta = \tan\theta_0 \exp\left(\frac{t}{2\tau}\right)$$

θ was the angle between the χ_3 axis and the z direction and τ^{-1} was the intrinsic rate of magnetic response defined in the previous section. This result indicated that the χ_3 axis moved from $\theta = \theta_0$ to $\theta = 0$ (the z direction) at the rate of $(2\tau)^{-1}$. While for the same particle, when exposed to a static field $\boldsymbol{B}$ in the z direction, behaved $\tan\theta = \tan\theta_0 \exp(-t/\tau)$, indicating that the χ_3 axis moved from $\theta = \theta_0$ onto the xy plane ($\theta = \pi/2$) at the rate of τ^{-1}. It

Table 1
Magnetic properties of the composite films prepared from different method at 298 K.

Condition	Sample	Hc[a] (Oe)		Ms[b] (emu/g)		Mr[c] (emu/g)	
		⊥	∥	⊥	∥	⊥	∥
Temperature	Natural drying	52.4	9.8	7.9	7.3	0.319	0.197
	Freeze drying	1.38	0.7186	2.756	2.933	4.125E−3	3.165E−3
Magnetic field	Static magnetic field	10.13	7.81	5.88	4.32	0.14	0.06
	Rotating magnetic field	0	0	0.91	0.88	0	0
Uniaxial drawing	DR = 1.04	45.6	30.9	7.9	4.1	0.283	0.725
	DR = 1.16	39.3	32.8	5.6	5.0	0.221	0.779
	DR = 1.22	13.3	16.8	5.9	4.9	0.212	0.468

[a] Coercivity.
[b] Saturated magnetization.
[c] Remnant magnetization.

further supported that the interesting rearrangement of the magnetic nanoparticles during the drying process under different conditions.

The different distribution of the magnetic nanoparticles in the composite film enabled it had different magnetic properties. Fig. 6 shows the magnetic hysteresis loop of the composite film tested at different directions. The composite film exhibited superparamagnetic behavior with extremely small hysteresis loops and coercivity in the direction that parallel or perpendicular to the applied field. The lack of hysteresis and coercivity was a characteristic of superparamagnetic particles and some single-domain particles. It was noted that there was no difference in the magnetic properties of the composite film that tested in the parallel or perpendicular to the applied field direction, indicating that the composite film prepared from rotating magnetic field had no magnetic anisotropy properties. It was agreed well with the TEM results, and further supported that there was a rearrangement of the magnetic nanoparticles in the composite film during the drying process.

In order to further clarify the rearrangement of the magnetic nanoparticles in the composite film during drying process, we tried to change the microstructure of the composite film by uniaxial drawing of the wet composite film with different draw ratios. The change in the microstructure of the cellulose film under different draw ratios has been reported in our previous work (Liu et al., 2009). We hope the changed microstructures of the cellulose matrix would hinder the rearrangement of the magnetic nanoparticles during the drying process, which would support our conclusion that there was a rearrangement happened to the magnetic nanoparticles during the drying process. Fig. 7 shows the TEM images of the composite film dried under different draw ratios. The distribution of the nanoparticles in the composite film was randomly even with a minor draw ratio, which was a little similar to that of the composite film prepared by freeze-dried. The morphology of the undrawn cellulose film could be depicted as a mixture of amorphous regions and crystalline domains, and the cellulose molecular chains arranged randomly in the films without drawing. In our previous works, the cellulose film exhibited stripes along the stretching direction, as a result of the orientation of the cellulose molecular clusters in the amorphous regions. Fibrils with width in a range of 200–400 nm were observed with spherical bumps in the range of 200 nm. The fibrillar morphology was established at the draw ratio of 1.04, whereas the spherical bumps changed the morphology. As the drawing proceeding, the orientation of the cellulose chains occurred dominantly in amorphous regions, which would destroy the microstructures of the cellulose matrix and hinder the rearrangement of the magnetic nanoparticles in the cellulose matrix during drying process. It was worth noting that particle size and morphology of the Fe_2O_3 nanoparticles changed under the uniaxial drawing process. When the draw rations was only 1.04, the Fe_2O_3 nanoparticles with particle size of about 34 nm and thickness about 10 nm were observed. With the increasing of the draw ratio to 1.22, the particle size of the Fe_2O_3 nanoparticles in the composite film increased to about 45 nm, and their thickness changed hardly, but their morphologies changed from plate-like to rod-like, as shown in Fig. 8d and h. While for the nanoparticles in the composite film dried at ambient conditions, the particle size and thickness was about 26 and 3 nm, respectively. It indicated that there was an obvious crystal growth of the Fe_2O_3 nanoparticles happened in the composite film under

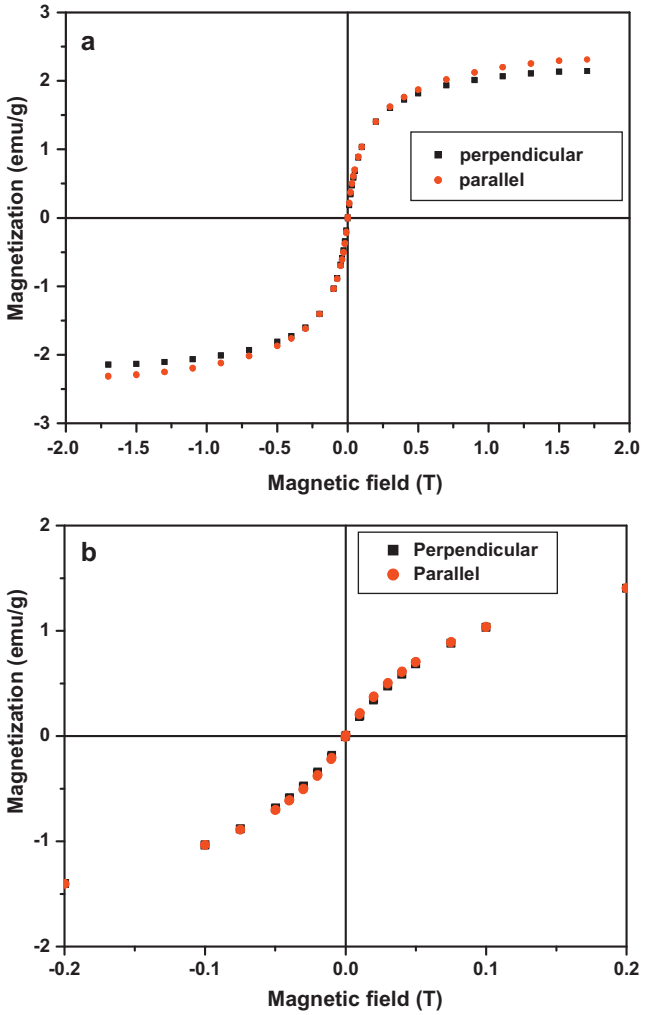

Fig. 6. Hysteresis loop of the air-dried composite film prepared from a rotating magnetic field measured at T = 298 K. (a) Full hysteresis loop and (b) the hysteresis loop between −200 and 200 Oe expanded.

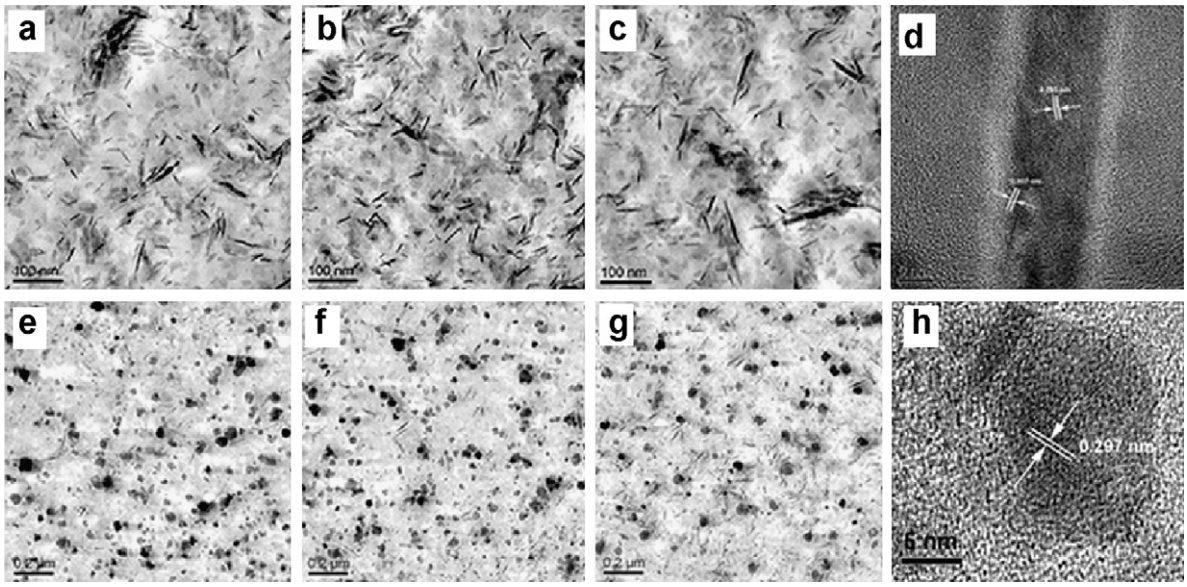

Fig. 7. TEM images of the composite films with draw ratios different from 1.04 to 1.22: (a–c) are the slices that perpendicular to the surface of the films, (e–g) are the slices that parallel to the surface of the films, d and e were HRTEM images of (c) and (g), respectively.

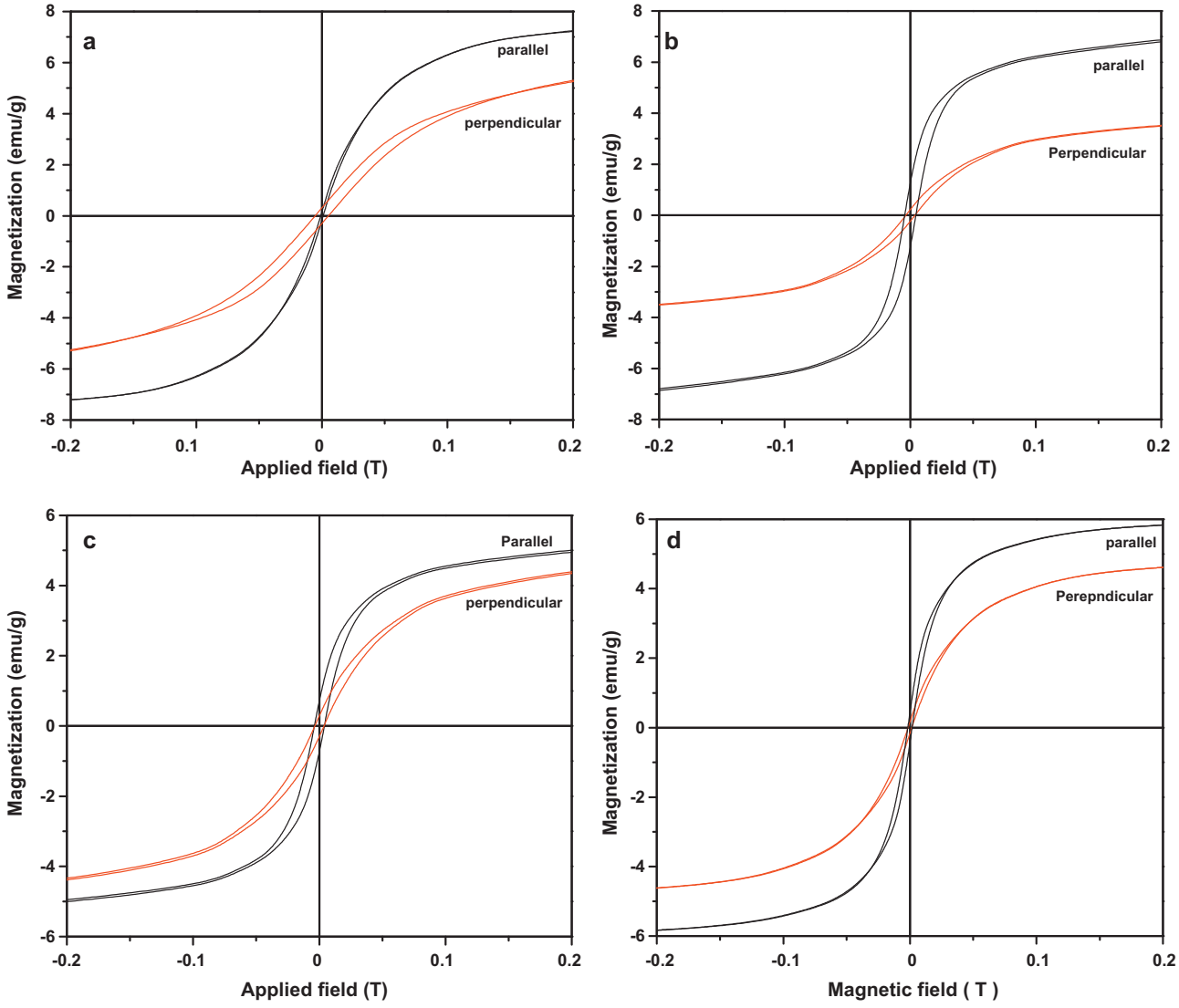

Fig. 8. Hysteresis loops of the composite films with different draw ratios measured at $T = 300$ K, (a) DR = 1.0; (b) DR = 1.04; (c) DR = 1.16; and (d) DR = 1.22.

uniaxial drawing process. It would be resulted from the deformation of the cellulose microstructure, which reduced the distance between Fe_2O_3 nanoparticles. Therefore, Fe_2O_3 nanoparticles that near to each other had an increased probability of touching each other, and particles formed in the deformed microstructures of the cellulose matrix during the drying process. All of the composite films exhibited weak magnetic behavior with small hysteresis loops and coercivity both in the parallel and perpendicularly applied fields, as it was shown in Fig. 8, and the magnetic properties were summarized in Table 1. The magnetic anisotropies of the composite films decreased with the increase of the draw ratios, because of the increase in the irregular arrangement of the magnetic nanoparticles. The composite film dried without uniaxial drawing had obviously magnetic anisotropy, the coercivity obtained from the perpendicular testing direction was about 52.4 emu/g, while in the parallel testing direction, it was only about 9.8 emu/g. The coercivities of the composite film with DR = 1.04 were about 45.6 and 30.9 emu/g for the perpendicular and parallel testing directions, respectively. The difference in the coercivities obtained from two different testing directions decreased with the increasing of the draw rations. The distribution of the Fe_2O_3 nanoparticles in the composite film was more and more randomly with the increase of the draw ratios, which was in good agreement with the TEM results. It further supported the conclusion that there was a rearrangement of the Fe_2O_3 nanoparticles in the composite film during the drying process. Moreover, it indicated that the magnetic properties of the composite film could be controlled by changing the preparation conditions.

4. Conclusions

Different preparation conditions could affect the structure and properties of the Fe_2O_3 nanoparticles synthesized in the cellulose composite films. The Fe_2O_3 nanoparticles in the cellulose matrix were plate-like and their distribution was randomly before drying. A weak magnetic field including static and rotating magnetic field has an obvious influence on the distribution of the Fe_2O_3 nanoparticles, but the distribution of the magnetic nanoparticles in the cellulose matrix was different. The uniaxial drawing of the composite film during the drying process destroyed the regular distribution of the Fe_2O_3 nanoparticles, leading to in the growth of the Fe_2O_3 nanoparticles with to the morphology of the nanoparticles changed from plate-like to rod-like. There was a rearrangement of the Fe_2O_3 nanoparticles during the drying process of the composite film at ambient conditions, the dipole–dipole interaction between magnetic nanoparticles and the microstructure of the cellulose matrix contributed to the regular distribution of the nanopatricles. The properties of the magnetic composite films could be controlled by changing the distribution of the Fe_2O_3 nanoparticles in the cellulose scaffolds.

Acknowledgements

This work was supported by National Basic Research Program of China (973 Program, 2010CB732203) and National Natural Science Foundation of China (51003043), and the Fundamental Research Funds for the Central Universities (JUSRP11107), as well as the goal-oriented project (JUSRP30905) of Jiangnan University.

References

Adelung, R., Aktas, O. C., France, J., Biswas, A., Kunz, R., Elbahri, M., et al. (2004). Strain-controlled growth of nanowires within thin-film cracks. *Nature Materials*, *3*, 375–379.

Akima, N., Iwasa, Y., Brown, S., Barbour, A. M., Cao, J., Musfeldt, J. L., et al. (2006). Strong anisotropy in the fat-infrared absorption spectra of stretch-aligned single-wall carbon nanotubes. *Advanced Materials*, *18*, 1166–1169.

Angelescu, D. E., Waller, J. H., Adamson, D. H., Deshpande, P., Chou, S. Y., Register, R. A., et al. (2004). Macroscopic orientation of block copolymer cylinders in single-layer films by shearing. *Advanced Materials*, *16*, 1736–1740.

Baker, B. M., Nathan, A. S., Gee, A. O., & Mauck, R. L. (2010). The influence of an aligned nanofibrous topography on human mesenchymal stem cell fibrochondrogenesis. *Biomaterials*, *31*, 6190–6200.

Bezryadin, A., Dekker, C., & Schmid, G. (1997). Electrostatic trapping of single conducting nanoparticles between nanoelectrodes. *Applied Physics Letters*, *71*, 1273–1275.

Bliznyuk, V. N., Singamaneni, S., Sanford, R. L., Chiappetta, D., Crooker, B., & Shibaev, P. V. (2005). Micro orientation and anisotropy of conductivity in liquid crystalline polymer films filled with carbon nanotubes. *Journal of Nanoscience Nanotechnology*, *5*, 1651–1655.

Chen, X. Q., Saito, T., Yamada, H., & Matsushige, K. (2001). Aligning single-wall carbon nanotubes with an alternating-current electric field. *Applied Physics Letters*, *78*, 3714–3716.

Chen, J.-P., Yang, P.-C., Ma, Y.-H., & Wu, T. (2011). Characterization of chitosan magnetic nanoparticles for in situ delivery of tissue plasminogen activator. *Carbohydrate Polymers*, *84*, 364–372.

Dykes, L. M. C., Torkelson, J. M., Burghardt, W. R., & Krishnamoorti, R. (2010). Shear-induced orientation in polymer/clay dispersions via in situ X-ray scattering. *Polymer*, *51*, 4916–4927.

Eguchi, M., Angelone, M. S., Yennawar, H. P., & Mallouk, T. E. (2008). Anisotropic alignment of lamellar potassium hexaniobate microcrystals and nanoscrolls in a static magnetic field. *Journal of Physical Chemistry C*, *112*, 11280–11285.

Goya, G. F., Berquo, T. S., Fonseca, F. C., & Morales, M. P. (2003). Static and dynamic magnetic properties of spherical magnetite nanoparticles. *Journal of Applied Physics*, *94*, 3520–3528.

Gu, H., Zheng, R. K., Zhang, X. X., & Xu, B. (2004). Using soft lithography to pattern highly oriented polyacetylene (HOPA) films via solventless polymerization. *Advanced Materials*, *16*, 1356–1359.

Hong, Y.-R., Adamson, D. H., Chaikin, P. M., & Register, R. A. (2009). Shear-induced sphere-to-cylinder transition in diblock copolymer thin films. *Soft Materials*, *5*, 1687–1691.

Kamat, P. V., Thomas, K. G., Barazzouk, S., Girishkumar, G., Vinodgopal, K., & Meisel, D. (2004). Self-assembled linear bundles of single wall carbon nanotubes and their alignment and deposition as a film in a dc field. *Journal of the American Chemical Society*, *126*, 10757–10762.

Kim, G. (2005). Thermo-physical responses of polymeric composites tailored by electric field. *Composites Science and Technology*, *65*, 1728–1735.

Kimura, T., Kimura, F., & Yoshino, M. (2006). Magnetic alteration of crystallite alignment converting power to a pesudo single crystal. *Langmuir*, *22*, 3464–3466.

Kimura, T., Yamato, M., Koshimizu, W., Koike, M., & Kawai, T. (2000). Magnetic orientation of polymer fibers in suspension. *Langmuir*, *16*, 858–861.

Kimura, T., & Yoshino, M. (2005). Three-dimensional crystal alignment using a time-dependent elliptic magnetic field. *Langmuir*, *21*, 4805–4808.

Kimura, T., Yoshino, M., Yamane, T., Yamato, M., & Tobita, M. (2004). Uniaxial alignment of the smallest diamagnetic susceptibility axis using time-dependent magnetic fields. *Langmuir*, *20*, 5669–5672.

Koerner, H., Jacobs, D., Tomlin, D. W., Busbee, J. D., & Vaia, R. D. (2004). Turing polymer nanocomposite morphology: AC electric field manipulation of epoxy-montomorillonite (clay) suspensions. *Advanced Materials*, *16*, 297–302.

Liu, S., Zhang, L., Sun, Y., Lin, Y., Zhang, X., & Nishiyama, Y. (2009). Supramolecular structure and properties of high strength regenerated cellulose films. *Macromolecular Bioscience*, *9*, 29–35.

Liu, S., Zhang, L., Zhou, J., & Wu, R. (2008). Nanocomposite fibers spun via an effective pathway. *Journal of Physical Chemistry C*, *112*, 4538–4544.

Liu, S., Zhang, L., Zhou, J., Xiang, J., Sun, J., & Guan, J. (2008). Fiberlike α-Fe_2O_3 macroporous nanomaterials fabricated by calcinating regenerate cellulose composite fibers. *Chemistry of Materials*, *20*, 3623–3628.

Liu, S., Zhou, J., & Zhang, L. (2011a). Effects of crystalline phase and particle size on the properties of plate-like Fe_2O_3 nanoparticles during γ to α-phase transformation. *Journal of Physical Chemistry C*, *115*, 3602–3611.

Liu, S., Zhou, J., & Zhang, L. (2011b). In situ synthesis of plate-like Fe_2O_3 nanoparticles in porous cellulose films with obvious magnetic anisotropy. *Cellulose*, *18*, 663–673.

Liu, S., Zhou, J., Zhang, L., Guan, J., & Wang, J. (2006). Synthesis and alignment of iron oxide nanoparticles in a regenerated cellulose film. *Macromolecular Rapid Communications*, *27*, 2084–2089.

Luo, X., Liu, S., Zhou, J., & Zhang, L. (2009). In situ synthesis of Fe_3O_4/cellulose microspheres with magnetic-induced protein delivery. *Journal of Materials Chemistry*, *19*, 3538–3545.

Luo, X., & Zhang, L. (2009). High effective adsorption of organic dyes on magnetic cellulose beads entrapping activated carbon. *Journal of Hazardous Materials*, *171*, 340–347.

Luo, X., & Zhang, L. (2010). Immobilization of penicillin G acylase in epoxy-activated magnetic cellulose microspheres for improvement of biocatalytic stability and activities. *Biomacromolecules*, *11*, 2896–2903.

Majewski, P. W., Gopinadhan, M., Jang, W.-S., Lutkenhaus, J. L., & Osuji, C. O. (2010). Anisotropic ionic conductivity in block copolymer membranes by magnetic field alignment. *Journal of the American Chemical Society*, *132*, 17516–17522.

Martin, C. A., Sandler, J. K. W., Windle, A. H., Schwarz, M. K., Bauhofer, W., Schulte, K., et al. (2005). Electric field-induced aligned multi-wall carbon nanotubes networks in epoxy composites. *Polymer*, *46*, 877–886.

Porion, P., Faugère, A. M., Michot, L. J., Paineau, E., & Delville, A. (2010). Orientational microdynamics and magnetic-field-induced ordering of clay platelets detected by using 2HNMR spectroscopy. *Langmuir*, *26*, 7035–7044.

Prasse, T., Cavaille, J. Y., & Bauhofer, W. (2003). Electric anisotropy of carbon nanofibre/epoxy resin composites due to electric field induced alignment. *Composite Science and Technology*, *63*, 1835–1841.

Quake, S. R., & Scherer, A. (2000). From micro-to nanofabrication with soft materials. *Science*, *290*, 1536–1540.

Shaver, J., Parra-Vasquez, A. N. G., Hansel, S., Portugall, O., Mielke, C. H., Ortenberg, M. V., et al. (2009). Alignment dynamics of single-walled carbon nanotubes in pulsed ultrahigh magnetic fields. *ACS Nano*, *3*, 131–138.

Shi, D., He, P., Lian, J., Chaud, X., Bud'ko, S. L., Beaugnon, E., et al. (2005). Magnetic alignment of carbon nanofibers in polymer. *Journal of Applied Physics*, *97*, 064312.

Smith, P. A., Nordquist, C. D., Jackson, T. N., Mayer, T. S., Martin, B. R., Mbindo, J. K. N., et al. (2000). Electric-field assisted assembly and alignment of metallic nanowires. *Applied Physics Letters*, *77*, 1399–1401.

Tai, X., Wu, G., Tominaga, Y., Asai, S., & Sumita, M. (2005). An approach to one-dimensional conductive polymer composites. *Journal of Polymer Science Part B: Polymer Physics*, *43*, 184–189.

Takahashi, T., Murayama, T., Higuchi, A., Awano, H., & Yonetake, K. (2006). Aligning vapor-grown carbon fibers in polydimethysiloxane using dc electric or magnetic field. *Carbon*, *44*, 1180–1188.

Tezvergil, A., Lassila, L. V. J., & Vallittu, P. K. (2003). The effect of fiber orientation on the thermal expansion coefficients of fiber-reinforced composites. *Dental Materials*, *19*, 471–477.

Wang, Z., Zhao, H., Lin, J., Zhuang, P., Yuan, W. Z., Hu, Q., et al. (2011). Chitosan rods reinforced by aligned multiwalled carbon nanotubes via magnetic-field-assistant *in situ* precipitation. *Carbohydrate Polymers*, *84*, 1126–1132.

Yamaguchi, A., Uejo, F., Yoda, T., Uchida, T., Tanamura, Y., Yamashita, T., et al. (2004). Self-assembly of a silica-surfactant nanocomposite in a porous alumina membrane. *Nature Materials*, *3*, 337–341.

Yanagihara, H., Hagiwara, J., Najazumi, M., & Kita, E. (2007). Dipole-induced magnetic anisotropy in γ-Fe_2O_3 (0 0 1) epitaxial films. *Applied Physics Letters*, *91*, 072508.

Zhou, J., Li, R., Liu, S., Li, Q., Zhang, L., Zhang, L., et al. (2009). Structure and magnetic properties of regenerated cellulose/Fe_3O_4 nanocomposite films. *Journal of Applied Polymer Science*, *111*, 2477–2484.